

Supporting Information for

Enhanced near-field coupling and tunable topological transition in hyperbolic van der Waals metasurfaces for optical nanomanipulation

Xueli Wang^a, Kaili Chang^a, Weitao Liu^a, Hongqin Wang^a, Junying Chen^a, Kaihui Liu^b,

Jianing Chen^c, Ke Chen^{a,*}

^a *Center for the Physics of Low-Dimensional Materials, School of Physics and Electronics, Henan University, Kaifeng, 475004, China*

^b *State Key Laboratory for Mesoscopic Physics, School of Physics, Peking University, Beijing, 100871, China*

^c *Institute of Physics, Chinese Academy of Sciences, Beijing, 100190, China*

*E-mail: kchen@henu.edu.cn

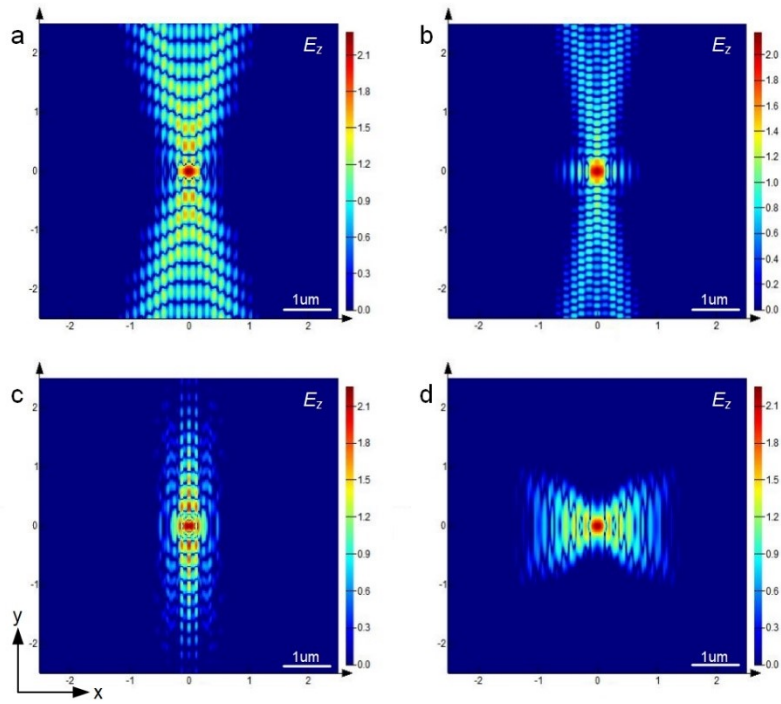


Fig.S1. The topological transition of polaritons in an iHBNG metasurface.

(a, b) The simulated near-field distributions E_z above the h-BN HMS (a, 1429 cm^{-1}) and graphene HMSs (b, 1272 cm^{-1}). (c, d) The simulated near-field distributions E_z above the iHBNG metasurface with different operation frequencies (c, $\omega = 1429 \text{ cm}^{-1}$, graphene chemical potential $\mu_c = 0.3 \text{ eV}$; d, 1272 cm^{-1} , $\mu_c = 0.6 \text{ eV}$).

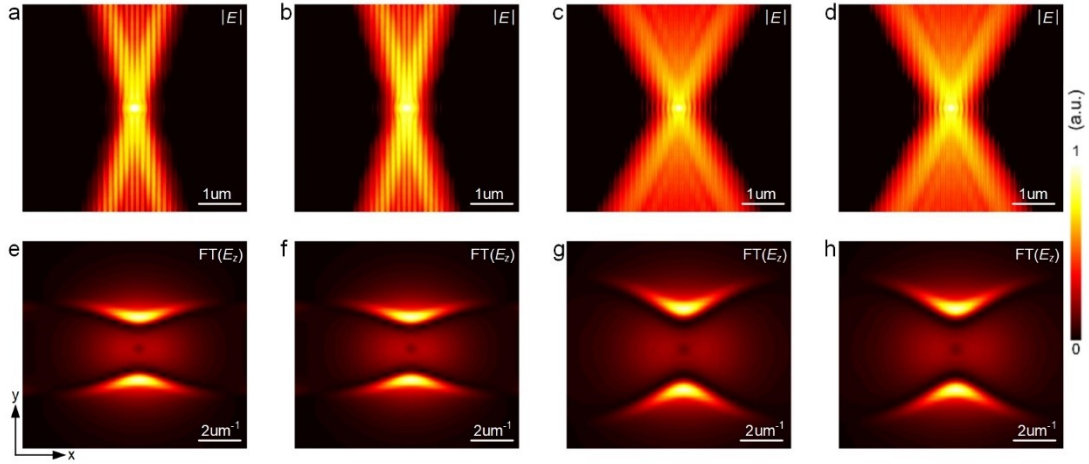


Fig.S2. Geometric-dependent near-field distributions of *h*-BN HMSs.

(a-d) The simulated magnitude of near-field distributions in the *h*-BN HMSs, $|E|$. The open angle of the isofrequency contour is 32° , 35° , 60° and 65° , respectively, at $W = 55$ nm (a), 60 nm (b), 65 nm (c), and 70 nm (d), $L = 120$ nm. (e-h) Absolute value of the corresponding Fourier transform (FT) of the simulated near-field distributions E_z at $W = 55$ (e), 60 (f), 65 (g), and 70 (h) nm, $L = 120$ nm.

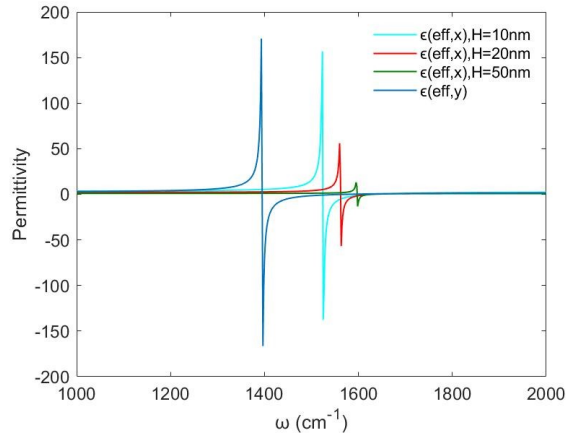


Fig.S3. The relationship between effective dielectric constant of hBN and thickness.

The blue line is the effective dielectric constant $\epsilon_{\text{eff},y}$, The green line is the effective dielectric constant $\epsilon_{\text{eff},x}$ of thickness $H=10\text{nm}$, The red line is the effective dielectric constant $\epsilon_{\text{eff},x}$ of thickness $H=20\text{nm}$, The cyan line is the effective dielectric constant

$\epsilon_{\text{eff},x}$ of thickness $H=50\text{nm}$.

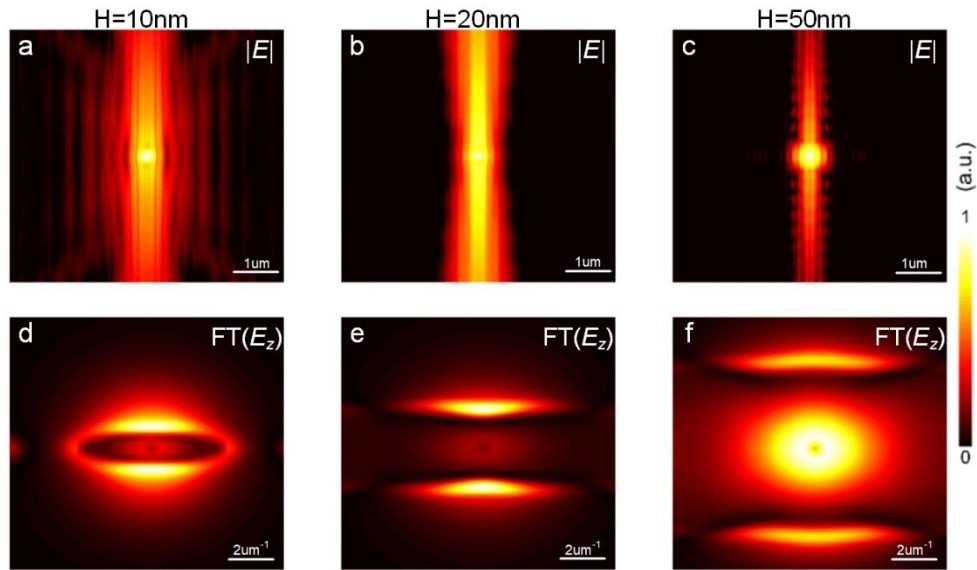


Fig.S4. Different thickness of *h*-BN results in topological transformation of heterojunction metasurfaces.

(a-c). The simulated magnitude of near-field distributions of iHBNG metasurfaces with the different thickness of h-BN of 10 (a), 20 (b), 50 (c) nm, $|E|$. (d-f) Fourier transform (FT) of the simulated near-field distributions E_z above the iHBNG metasurfaces with different thickness of h-BN of 10 (a), 20 (b), 50 (c) nm.

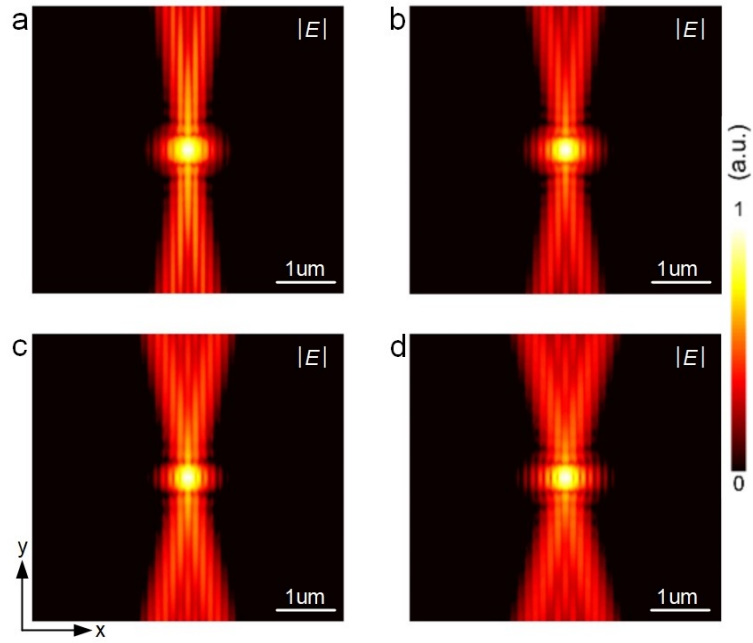


Fig.S5. Geometric-dependent near-field distributions of graphene metasurfaces.

(a-d) The simulated magnitude of near-field distributions in the graphene metasurfaces, $|E|$. The open-angle of the isofrequency contour is 10° , 15° , 18.9° , and 26.8° , respectively, at $G = 50$ (a), 55 (b), 60 (c), and 65 (d) nm, $L = 120$ nm.

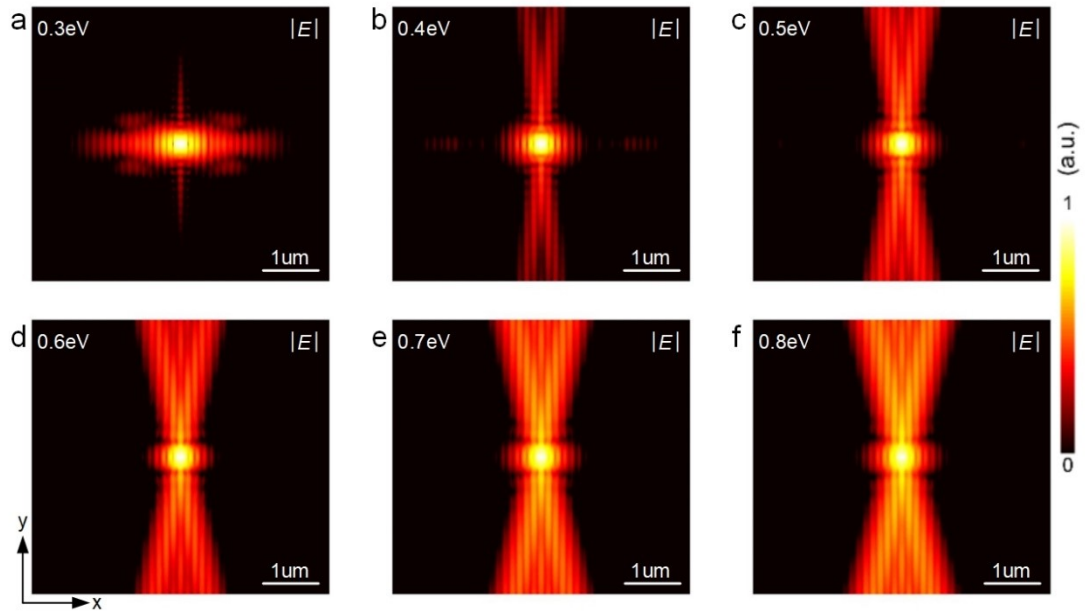


Fig.S6. Chemical potential-dependent tunability of graphene hyperbolic plasmons and their topological transitions.

(a-f) Simulated magnitude of the near-field distributions above the graphene metasurfaces with the chemical potentials of 0.3 (a), 0.4 (b), 0.5 (c), 0.6 (d), 0.7 (e), 0.8 (f) eV, $|E|$. $L = 120$ nm, $W = 60$ nm.

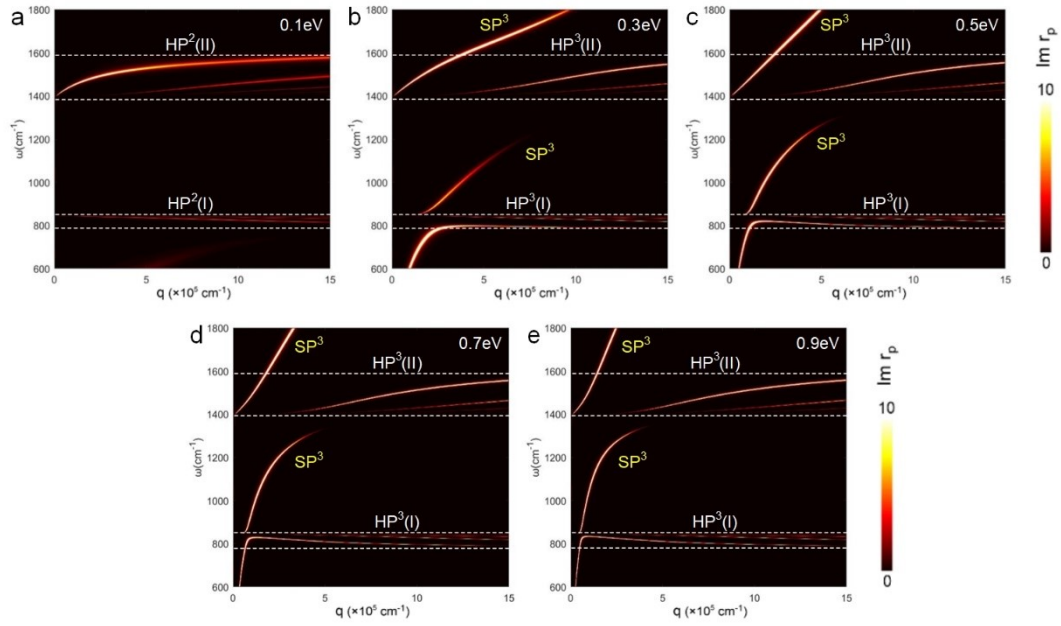


Fig.S7. Calculated HP^3 and SP^3 dispersion of the heterostructure of monolayer graphene/ h -BN slab by Fresnel reflection coefficient r_p .

(a-e) at the chemical potentials of 0.1 (a), 0.3 (b), 0.5 (c), 0.7 (d), 0.9 (e) eV.

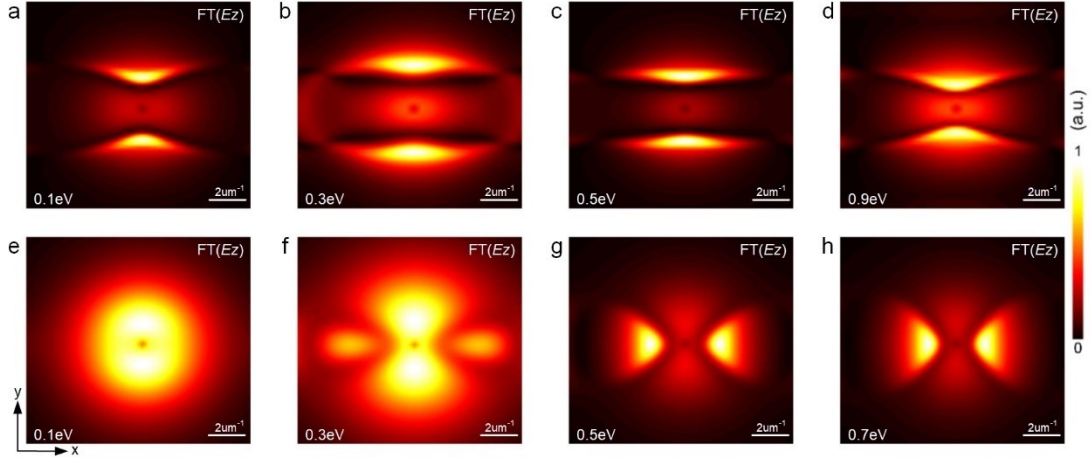


Fig.S8. The absolute value of the corresponding Fourier transform (FT) of the simulated near-field distributions E_z above the iHBNG metasurface with different graphene chemical potential.

(a-d) Fourier transform (FT) of the simulated near-field distributions E_z above the iHBNG metasurfaces at $\omega = 1429 \text{ cm}^{-1}$ with different chemical potentials, $|E|$. $\mu_e = 0.1, 0.3, 0.5,$ and 0.9 eV . (e-h) Fourier transform (FT) of the simulated near-field distributions E_z above the iHBNG metasurfaces at $\omega = 1272 \text{ cm}^{-1}$ with different chemical potentials, $|E|$. $\mu_e = 0.1, 0.3, 0.5,$ and 0.7 eV .

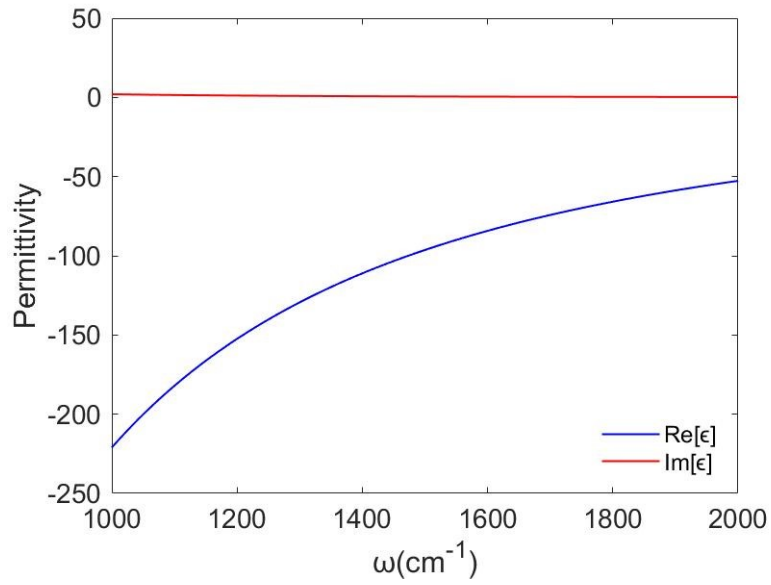


Fig.S9. The permittivity of graphene $\mu_e = 0.6$ eV calculated by the surface conductivity. The blue (red) line represents the real (imaginary) part of permittivity ($\sigma(\omega)$).

Supplementary Note 1. The choice of design thickness of *h*-BN slabs.

In our model, We considered three main factors. First, the thickness of *h*-BN causes the variation of hyperbolic phonon polaritons dispersion. As the thickness of *h*-BN increases, the momentum of the phonon polariton decreases¹. Thus, the large mismatch of momentum between graphene plasmons and hyperbolic phonon polaritons leads to their weak coupling. Second, according to the effective dielectric constant of *h*-

BN nonlocal correction parameter $\varepsilon_c = \frac{2L}{\pi h} \ln \left[\csc \left(\frac{\pi \xi}{2} \right) \right]$, the relationship between

effective dielectric constant and thickness is calculated in Fig.S3. As the thickness increases from 10 to 50 nm, the resonant frequency related to the effective dielectric constant $\varepsilon_{\text{eff},x}$ shows a blue shift from ~ 1523 to ~ 1600 cm^{-1} . Further, the near-field distributions and the related Fourier transforms of the iHBNG metasurfaces with the *h*-BN thicknesses of 10, 20, and 50 nm, are simulated as shown in Fig.S4, and the elliptic dispersion at frequency 1402, 1429, and 1482 cm^{-1} are exhibited, respectively. These results are consistent with the simulation of the effective dielectric constant at different thickness of *h*-BN. From above analysis, we conclude that the near-field distribution of iHBNG metasurfaces is more suitable when the *h*-BN thickness is set to be 20 nm. In addition, the over large *h*-BN thickness is indeed not essential for the propagation and modulation of polaritons along the metasurfaces, which will improve the difficulty in the actual sample preparation and lithography. Considering above factors, we have chosen an optimal thickness of the *h*-BN slab (20 nm) in the design of iHBNG metasurfaces.

Supplementary Note 2. The ratio in geometrically structural matching between graphene and *h*-BN ribbons.

In our text, We set the 1:1 representative model. Firstly, this ratio can realize the coupling of *h*-BN hyperbolic phonon polaritons and graphene plasmons to retain the minimum coupling losses. Secondly, according to our discussion in manuscript and supporting information in Fig S2 and S5, different structures will cause different propagation angles and field distributions of polaritons in the plane. This is due to the change of the structure will lead to frequency of effective permittivity $\epsilon_{\text{eff},x}$ in *h*-BN metasurfaces and effective conductivity $\text{Im}\sigma_x$ in graphene metasurfaces change. In addition, the symmetrical proportion is easy to manufacture and can minimize the uncertainty of manufacturing. The effective regulation of polaritons can be achieved when the two structures are kept at 1:1.

Supplementary Note 3. Dispersion of hybridized plasmon–phonon–polaritons.

In our theoretical model, we derive the dispersion relation of hybridized plasmon-phonon-polaritons based on macroscopic electromagnetic theory.² For simplicity, we just analyze the formulas of the *h*-BN/graphene heterostructures to reveal the polaritons coupling mechanism without considering the interstrip non-local effect. In general, a versatile air/graphene/*h*-BN/graphene/SiO₂ structure is utilized as an infinite stratified medium to illustrate our calculation methods,³ which consists of three regions: region 1 ($z < 0$, air), region 2 ($0 < z < d$, *h*-BN), and region 3 ($z > d$, substrate), where d is the thickness of the *h*-BN slab. For TM (p -polarized) waves, we can set the magnetic fields in each region as,

$$\bar{H}_1 = \hat{y}e^{iqx}(A_+ e^{+ik_{1z}z} + A_- e^{-ik_{1z}z}) \quad (3)$$

$$H_2 = \hat{y}e^{iqx}(B_+ e^{+ik_{2z}z} + B_- e^{-ik_{2z}z}) \quad (4)$$

$$H_3 = \hat{y}e^{iqx}(C_+ e^{+ik_{3z}z} + C_- e^{-ik_{3z}z}) \quad (5)$$

We can plug $(\hat{x}q + \hat{x}k_z) \times \bar{H} = -\epsilon\omega\bar{E}$ into the above equations to get the corresponding electric fields E for each region.

Furthermore, the wavevector components perpendicular to the interface are listed as below,

$$k_{z1} = \sqrt{\frac{\omega^2}{c^2}\epsilon_{r1} - q^2} \quad (6)$$

$$k_{z2} = \sqrt{\frac{\omega^2}{c^2} \epsilon_x - q^2 \frac{\epsilon_x}{\epsilon_z}} \quad (7)$$

$$k_{z3} = \sqrt{\frac{\omega^2}{c^2} \epsilon_{r3} - q^2} \quad (8)$$

where ϵ_{r1} and ϵ_{r3} are the relative permittivities of regions 1 and 3 media, respectively.

By setting the surface normal $\hat{n} = -\hat{z}$ at $z = 0$, we obtain,

$$\hat{n} \times (\mathbf{E}_1 - \mathbf{E}_2) = 0 \quad (9)$$

$$\hat{n} \times (\mathbf{H}_1 - \mathbf{H}_2) = \hat{x} \sigma_{s1} E_{x1} \quad (10)$$

and at $z = d$, we obtain,

$$\hat{n} \times (\mathbf{E}_2 - \mathbf{E}_3) = 0 \quad (11)$$

$$\hat{n} \times (\mathbf{H}_2 - \mathbf{H}_3) = \hat{x} \sigma_{s2} E_{x2} \quad (12)$$

Here we denote the surface conductivity of the upper and lower graphene layers as σ_{s1} and σ_{s2} ,⁴ respectively. When the electromagnetic wave is incident from region 3, we

obtain: $\frac{C_+}{C_-} = \mathcal{R}_{32}$,

$$R_p = \mathcal{R}_{32} = R_{32} + \frac{T_{32} R_{21} T_{23} e^{+i2k_{z2}d}}{1 - R_{21} R_{23} e^{+i2k_{z2}d}} \quad (13)$$

$$R_{32} = \frac{1 + \frac{\sigma_{S2} k_{z2}}{\omega \varepsilon_0 \varepsilon_x} - \frac{k_{z2}/\varepsilon_x}{k_{z3}/\varepsilon_{r3}}}{1 + \frac{\sigma_{S2} k_{z2}}{\omega \varepsilon_0 \varepsilon_x} + \frac{k_{z2}/\varepsilon_x}{k_{z3}/\varepsilon_{r3}}}, \quad R_{23} = \frac{1 + \frac{\sigma_{S2} k_{z3}}{\omega \varepsilon_0 \varepsilon_{r3}} - \frac{k_{z3}/\varepsilon_{r3}}{k_{z2}/\varepsilon_x}}{1 + \frac{\sigma_{S2} k_{z3}}{\omega \varepsilon_0 \varepsilon_{r3}} + \frac{k_{z3}/\varepsilon_{r3}}{k_{z2}/\varepsilon_x}},$$

In the above, we have

$$R_{21} = \frac{1 + \frac{\sigma_{S1} k_{z1}}{\omega \varepsilon_0 \varepsilon_{r1}} - \frac{k_{z1}/\varepsilon_{r1}}{k_{z2}/\varepsilon_x}}{1 + \frac{\sigma_{S1} k_{z1}}{\omega \varepsilon_0 \varepsilon_{r1}} + \frac{k_{z1}/\varepsilon_{r1}}{k_{z2}/\varepsilon_x}}, \quad T_{32} = \frac{2}{1 + \frac{\sigma_{S2} k_{z2}}{\omega \varepsilon_0 \varepsilon_x} + \frac{k_{z2}/\varepsilon_x}{k_{z3}/\varepsilon_{r3}}}, \quad T_{23} = \frac{2}{1 + \frac{\sigma_{S2} k_{z3}}{\omega \varepsilon_0 \varepsilon_{r3}} + \frac{k_{z3}/\varepsilon_{r3}}{k_{z2}/\varepsilon_x}},$$

where ε_0 is the permittivity of free space.

Therefore, we can finally solve the dispersion of the air/hBN-graphene/substrate structure by setting $\sigma_{S1} = 0$.

REFERENCES

1. I. Dolado, F. J. Alfaro-Mozaz, P. Li, E. Nikulina, A. Bylinkin, S. Liu, J. H. Edgar, F. Casanova, L. E. Hueso, P. Alonso-González, S. Vélez, A. Y. Nikitin, R. Hillenbrand, *Adv. Mater.* 2020, **32**(9),1906530.
2. J. A. Kong, *Electromagnetic Wave Theory*, EMW Publishing, Cambridge, MA, 2008.
3. X. Lin, Y. Yang, N. Rivera, J. J. López, Y. Shen, I. Kaminer, H. Chen, B. Zhang, J. D. Joannopoulos, M. Soljačić, *Proc. Natl. Acad. Sci.*, 2017, **114**, 6717–6721.
4. X. Guo, H. Hu, X. Zhu, X. Yang, Q. Dai, *Nanoscale*, 2017, **9**, 14998–15004.